Werk

Jahr: 1982
Kollektion: fid.geo
Signatur: 8 Z NAT 2148:51
Digitalisiert: Niedersächsische Staats- und Universitätsbibliothek Göttingen
Werk Id: PPN1015067948_0051
PURL: http://resolver.sub.uni-goettingen.de/purl?PPN1015067948_0051

LOG Id: LOG_0038
LOG Titel: Shear fracture development and seismic regime in pyrophyllite specimens with soft inclusions
LOG Typ: article

Übergeordnetes Werk

Werk Id: PPN1015067948
PURL: http://resolver.sub.uni-goettingen.de/purl?PPN1015067948
OPAC: http://opac.sub.uni-goettingen.de/DB=1/PPN?PPN=1015067948

Contact

Niedersächsische Staats- und Universitätsbibliothek Göttingen
Georg-August-Universität Göttingen
Platz der Göttinger Sieben 1
37073 Göttingen
Germany
Email: gdz@sub.uni-goettingen.de

J Geophys (1982) 51:180–187

Journal of Geophysics

Shear Fracture Development and Seismic Regime in Pyrophyllite Specimens with Soft Inclusions

G. Sobolev[1] and F. Rummel[2]

[1] Institute of Physics of the Earth, Academy of Sciences, Moscow, USSR
[2] Institute of Geophysics, Ruhr-University Bochum, P.O. Box 102148, D-4630 Bochum 1, Federal Republic of Germany

Abstract. The paper describes the sequence of fracture development in pyrophyllite specimens containing a soft inclusion. The inclusions were induced by drilling a number of small boreholes into the central part of the specimens. It is assumed that the soft inclusion models a crustal earthquake source region. The specimens were deformed uniaxially using a servo-controlled loading system, which permitted controlled fracturing from initial cracking to final specimen collapse. The transition from pre-peak randomly distributed cracking to the formation of macro-shear fractures is characterized by a critical crack density and can be defined by a unique critical crack interaction parameter, which appears to be material-insensitive. The tests also permitted us to estimate intrinsic fracture mechanics parameters for mode-II fracture: For the critical energy release rate G_{IIC} an average value of 8.3 $kJ \cdot m^{-2}$, for the critical stress intensity factor K_{IIC} an average value of 4.2 $MNm^{-3/2}$ were obtained. Both visual observation and the analysis of acoustic emission activity demonstrate that fracture in rock specimens is characterized by seismic patterns similar to those known from active earthquake regions, i.e. seismic gaps and periods of seismic silence.

Introduction

Seismological data such as the seismic radiation pattern around earthquake-epicenters demonstrate that crustal earthquakes are the result of macroscopic dynamic shear fractures. Consequently, in a theoretical approach, the process of earthquake rupture is modelled as the development of a displacement disconituity on a plane surface, either by the use of simple dislocation-type models (Haskell, 1964; 1966) or by using shear-crack-like models (Kostrov, 1975; Madariaga, 1976; 1977; Rudnicki, 1980). A comprehensive review on this subject is presented by Rice (1980).

In comparison, the present understanding of the deformation processes precursory to earthquake rupture and associated with the longterm earthquake preparation is qualitative and speculative. Since these processes may be significant to earthquake prediction research, the need for further work in this area is obvious. Laboratory research on fracture processes in rocks under controlled environmental conditions, in particular, may provide intrinsic fracture mechanics parameters as well as allow a qualitative discrimination of various fracture processes in the sequence of fracture development in space and time.

Here we present some results from simple fracture tests on pyrophyllite specimens which contain soft inclusions as an analogy for an earthquake source region. The tests are carried out to demonstrate the complete fracture process from initial micro-fracturing within the soft inclusion region to the development of a macroscopic shear fracture.

Qualitative Models of Earthquake Preparation

Existing models of earthquake preparation are derived primarily from field observations in seismo-active regions, which include e.g. seismological characteristics, fault creep, pore pressure changes, and physical rock property alterations. Significant contributions also came from rock mechanics experimental research, particularly from experiments in stiff or servo-controlled testing systems (e.g. Rummel, 1970; 1975).

Such experiments permit controlled fracturing and also provide relevant fracture data for theoretical models (Rummel et al., 1978; Rice, 1980). One impetus for the theoretical approach was the application of fracture mechanics.

Most of the existing models of earthquake prediction are reviewed by Myachkin et al. (1975) or by Rice (1979). They differ as to the emphasis which is put on either volumetric cracking in "intact" rock, premonitory micro-fracturing in the vicinity of existing faults, time dependent fracture mechanisms, or the importance of migrating pore fluids. The stick-slip model e.g. (Brace and Byerlee, 1966) neglects premonitory dilatancy and only takes into consideration the most advanced stage of earthquake preparation, namely frictional slip along existing shear surfaces.

Since all models to a certain extent take into account the heterogeneity of the earth's crust which includes the coexistence of rocks with different deformation behaviour and strength, as well as the spatial distribution of existing fractures of various dimensions, we may derive the following general concept of the earthquake preparation process: Due to crustal heterogeneity we may expect a non-uniform statial distribution of the stress field. Then, during tectonic strain energy accumulation the first stage of earthquake source preparation will be characterized by quasi-static crack growth at locations of high stress concentration. This fracturing should occur preferentially in crustal regions consisting of weaker or softer rocks. Initially it will be ran-

Offprint requests to: F. Rummel

0340-062X/82/0051/0180/$01.60

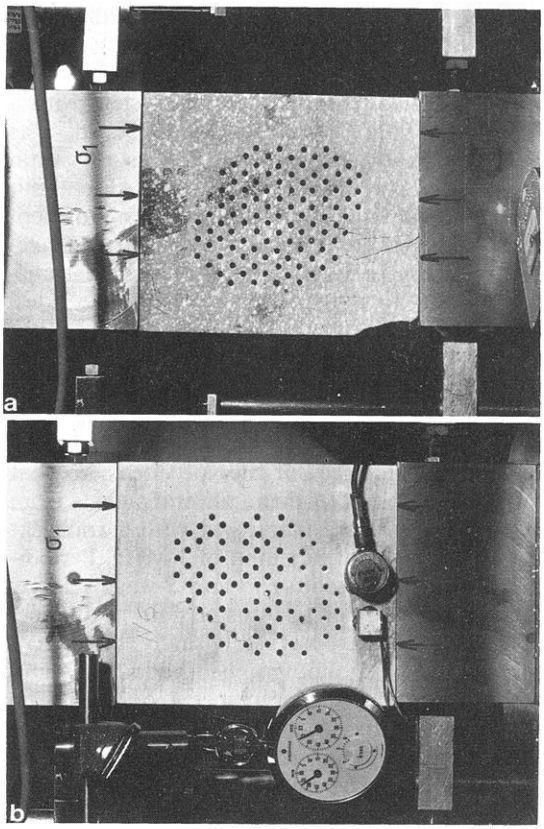

Fig. 1 a and b. Common view of pyrophyllite specimens with elliptical soft inclusions after determination of fracture experiments. For better crack detection specimen faces are painted with chalk **b**

domly distributed over a large volume and will cause dilatancy that may lead to precursory phenomena. During the subsequent stage crack interaction will occur in areas where the crack density approaches a critical value. This will induce crack coalescence and will lead progressively to the development of macroscopic shear fractures (Myachkin et al., 1974). Instability will occur if the available strain energy exceeds the energy demand for stable fracture growth.

At present the major problem in this general model is to theoretically describe the transition from volumetric fracturing to macroscopic fault formation. This process is known from seismological observations before several earthquakes e.g. for the 1975 Haicheng earthquake (Hsu, 1976; see also Talwani, 1981), but was not observed e.g. for earthquakes in the Garm region (Nersesov et al., 1979).

The model also does not explicitly explain seismological phenomena such as the existence of seismic gaps or seismic silence prior to main shocks.

One possible theoretical approach to addressing the problem of fault formation on the basis of continuum mechanics is presented by Rice (1980). It consists of seeking conditions "under which uniform patterns of deformation become unstable in the sense that bifurcation of continuing deformation into a localized shear bands becomes possible". An alternative possibility is to assume nonuniform crack distribution and crack interaction in areas with a critical crack density as mentioned above (Myachkin et al., 1974). This process was experimentally investigated for polymers, metals and some single crystals by Zhurkov et al. (1977). The experiments revealed that the critical stage when tensile cracks begin to coalesce can be specified by only one empirical statistical parameter, which seems to be material insensitive. This parameter may be called critical crack interaction parameter K[1] and is defined as $K = \tilde{L}/\bar{l}$, where $\bar{l}$ is the average crack length, and $\tilde{L}$ is the average nearest distance between neighbouring cracks. $\tilde{L}$ is proportional to the number of cracks per unit volume ($\tilde{L} \sim n^{-1/3}$). K ranges from 3 to 5 for all materials tested.

So far, no measurements of K-values have been conducted for shear failure in rocks, although the transition from micro-fracturing to shear fracture formation in rock was carefully examined by several investigators (e.g. Wawersik, 1968; Mogi, 1968; Lockner and Byerlee, 1977; Sobolev et al., 1978). An attempt to measure K for seismoactive faults showed K-values of 6–8 for the Kamchatka seismic region (Sobolev and Zavialov, 1981).

Specimen Specifications and Testing Procedure

Pyrophyllite specimens were chosen for the experiments since this rock is less brittle than most crystalline rocks. Therefore experiments even under unconfined room temperature loading conditions allow us to observe the total sequence of fracture development. The relevant mechanical properties of this rock were determined earlier by Sobolev et al. (1978).

The specimens were rectangular prisms with a loading area of about $(4 \times 10)\,\mathrm{cm}^2$ and a height of 10–14 cm. In order to both induce stress concentrations as well as simulate a soft inclusion within a relatively stiff surrounding rock mass, a number of small holes of 2.5 mm diameter were drilled into the central part of the large faces of each specimen (Figs. 1 and 2). The holes were left open or were filled with epoxy (Araldit E-HY 951). The soft inclusion is represented by the total region containing drillholes. The shape of the inclusion was either circular, elliptical or rectangular.

The effect of stress concentration on the fracture development around circular holes in rock specimens was extensively investigated by Rummel (1975) and Sobolev et al. (1980). Such tests show tensile crack initiation at the holes at the location of maximum induced tensile stress. Such cracks become stable at close distances from the hole.. Further cracking in the vicinity of the hole is generally complex.

The state of stress and strain within a homogeneous inclusion in an infinite region can be calculated from the far-field stresses and the elastic properties of the inclusion and the surrounding material. Solutions for the case of circular or elliptical inclusions will be found in Muskhelishvili (1953). For our case, elliptical soft inclusions consisting of a region with drillholes as shown in Fig. 1, a rough estimation of the induced average stress-field inside the inclusion due to uniaxial loading was given by Kostrov (private communication). The ratio between the effective shear moduli inside and outside of the inclusion is about 0.87, resulting in an internal maximum principal stress of about 90% and an internal minor principal stress (tension) of about 5% of the externally applied uniaxial stress. The direction of the average maximum compression inside the inclusion only deviates from the direction of the applied load by an angle

1 The symbol K for the critical crack interaction parameter was used by Zhurkov et al. It should be distinguished from the stress intensity factor K_{II} used later in this paper

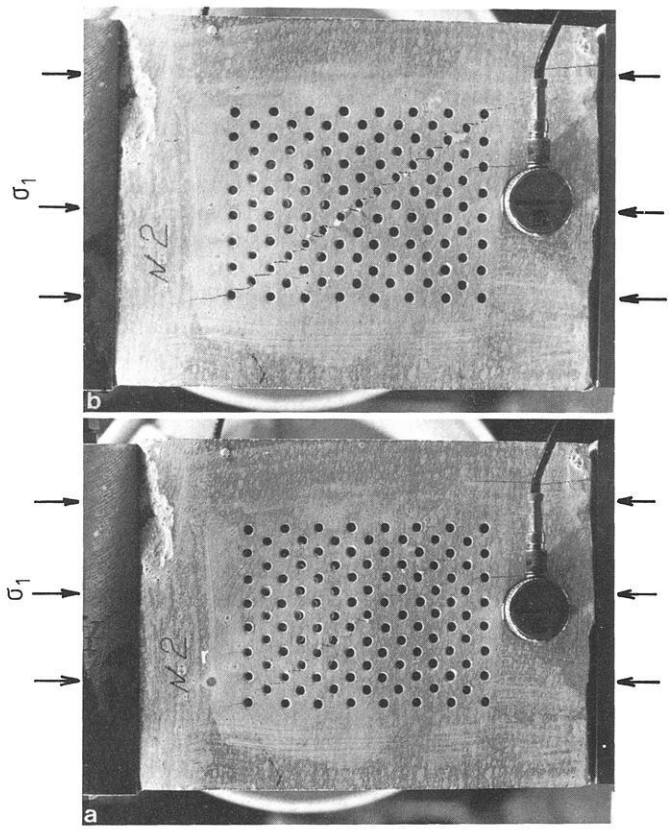

Fig. 2a and b. Example of a macro-shear fracture development in pyrophyllite along the main diagonal in the soft inclusion. **a** shear fracture partly developed with some unbroken barriers, **b** fully developed 7 min later

less than 1%. Although no estimation exists for rectangular soft inclusions we assume that the deviations from the stress in the surrounding material are also small.

All data for the 15 specimens tested are included in Table 1. Three specimens of smaller size were tested to estimate the strength reduction as a result of the number of holes. One specimen was without holes. The rest of the specimens contained 28–113 holes. In two samples all holes, in one sample only 70% of the holes were filled with epoxy. All specimens were ground parallel to within ± 0.05 mm.

The specimens were uniaxially compressed in a 60 ton capacity servo-controlled hydraulic loading system with a response time of less than 5 ms (Rummel, 1975). All tests except one (No. 3) were carried out at a constant strain rate of $\dot{\varepsilon} = 3.10^{-6}\ s^{-1}$. Specimen No. 3 was loaded to about 90% of its maximum strength and then the stress was kept constant. Axial strain of the specimen or piston displacement was measured by two inductive displacement transducers placed parallel to the specimen on opposite sides. Both axial stress and axial strain were monitored continuously on paper recorders. Acoustic emission activity was picked-up by piezo-electric transducers (Panametrix) and registered via amplifiers and a pulse counter parallel to stress and strain. In most cases the transducers were placed diagonally on both large faces of the specimens, so that the inclusion area was between them. Several signals from acoustic emission events were monitored with a transient recorder with an upper frequency limit of 1 MHz. Periodically, the transducers were used for *P*- and *S*-wave velocity measurements using the pulse-transmission technique. Fracture development was observed visually through a magnifying lense, and both photographed periodically and filmed at a frequency of one picture per 1 or 2.5 s. The photos permitted a quantitative evaluation of visible cracks on the surface as a function of time, the film allowing us to observe the speed of fracture development.

Progressive Fracture Development

During initial loading the pyrophyllite specimens deformed approximately linearly with stress. This results in a Young's modulus of $E = 2.3$ GPa for the intact rock (Specimen No. 7) and in an average effective Young's modulus of $E_{eff} = 1.8$ GPa for the specimens containing a soft inclusion. In comparison, the theoretical estimation by Kostrov yields a reduction of the effective Young's modulus due to the soft inclusion of only 4%.

First fracturing appeared at a stress σ_f of about 75% of the maximum strength σ_m and generally was confined only to the soft inclusion (Table 1). It occured in the formation of axially oriented tensile cracks which initiated at the

Table 1. Specimen dimensions and physical properties (N number of holes, σ_m uniaxial strength, σ_f stress at first visible fracture, ε axial strain at σ_m, ε_f strain at σ_f, E_{eff} effective Young's modulus, K critical crack interaction parameter)

Specimen number	Size cm	Shape of inclusion	N	Type of holes	σ_m MPa	σ_f/σ_m	ε %	$\varepsilon_f/\varepsilon$	E GPa	K
A	4 × 4 × 4	–	–	–	32.5					
B	4 × 4 × 4	rectangular	5	empty	28.0					
C	4 × 4 × 4	rectangular	14	empty	23.0					
7	10 × 7.4 × 4.5	–	–	–	23.8	0.86	1.3	0.70	2.3	–
1	14 × 10 × 4.5	rectangular	113	empty	14.7	0.54	1.2	0.36	1.8	3.4
2	13.5 × 10 × 4.5	rectangular	113	empty	11.6	0.93	0.87	0.86	1.6	5.0
4	14 × 10 × 4.5	rectangular	113	empty	14.2	0.80	1.1	0.73	1.4	4.1
5	12 × 10 × 4.5	elliptical	105	empty	18.5	0.69	1.0	0.62	2.1	3.5
6	12 × 10 × 4.5	elliptical	78	empty	13.7	0.86	0.97	0.82	1.5	5.4
9	14 × 10 × 4.5	elliptical	28	empty	11.5	0.79	1.13	0.71	1.1	5.5
8	12 × 10 × 4.5	elliptical	105	epoxy	13.4	0.79	0.93	0.69	1.7	3.3
10	13 × 10 × 4.5	circular	70	epoxy	18.7	0.66	1.55	0.52	1.5	3.2
12	11.5 × 10 × 4.5	circular	60	30% empty 70% epoxy	14.2	0.43	1.27	0.34	1.4	3.2
3	14 × 10 × 4.5	rectangular	113	empty	–	–	–	–	2.4	–

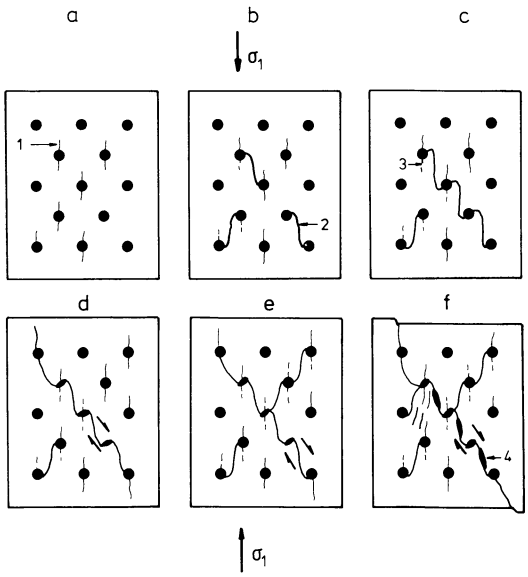

Fig. 3a–f. Sequence of fracture development in soft inclusions consisting of holes (schematically). 1 tensile cracks, 2 shear-like cracks, 3 closed tensile cracks, 4 opening of macro-shear fracture sections: **a** tensile crack accumulation; **b** crack interaction by shear-like cracks; **c** macro-shear fracture formation; **d** continuation of crack accumulation during a period of shear fracture stability; **e** appearance of further macro-fractures and their interaction; **f** micro-cracking in regions of high compression prior to macro-fracture instability

locations of maximum induced tensile stresses around the drillholes, and propagated over a distance of only about one hole-diameter away from the hole. Crack initiation and crack growth during this stage was not associated with acoustic emission activity which could be detected with the recording system (machine noise). The distribution of these cracks was approximately random over the total area of the inclusion. Generally, about 10–20 of such cracks could be identified.

The formation of a diagonal shear fracture initiates near the peak strength by the growth of inclined cracks around the holes, which interact with each other. Generally, this interaction occurs simultaneously in the vicinity of diagonally neighboured holes and is accompanied both by a rapid stress drop and acoustic emission activity. A typical sequence of this type of shear fracture development is shown in Fig. 2. During a first stage the shear fracture passes through holes along the main diagonal in the upper and central part of the specimen leaving three unbroken bridges in the bottom right and the upper left region of the soft inclusion (Fig. 2a). In a later stage (7 min after the first event) the shear fracture has almost fully developed along the diagonal within the soft inclusion (Fig. 2b). Other experiments show the formation of several shear fractures which develop subsequently. A new shear fracture usually stops when it interacts with an existing old fracture. Generally, tensile cracking is absent during the growth of one shear fracture, but may occur again in an unfractured region as preparation for a subsequent macro-shear fracture.

The mechanisms and the sequence of fracturing process observed in pyrophyllite specimens with soft inclusions are schematically summarized in Fig. 3. The plot will also emphasize that the macro-shear fractures do not originate directly by interaction of tensile cracks, which developed during the first stage of fracturing. The effect of closure of tensile cracks by shear fractures, the stopping of shear fractures at intersections, and the breaking of barriers are clearly demonstrated. In Fig. 4 some examples of typical stress-strain curves are presented. The average strength of the pyrophyllite specimens follows the empirical relation

$$\bar{\sigma}_N = \bar{\sigma}_0 - a \log N \tag{1}$$

where $\bar{\sigma}_0$ is the average strength of intact specimens, $\bar{\sigma}_N$ is the strength of specimens containing N holes within a soft inclusion region, and $a = 8$ MPa.

Preparation of Macro-Shear Fractures

A detailed picture of the development of the macro-shear fracture is obtained if we consider the distribution of cracks in space (or surface area) and time. This is demonstrated for Specimens No. 2 and No. 1 in Figs. 5 and 6, where all crack events associated with the formation of the main shear fractures are plotted as a function of time t (or strain ε) and the location along the narrow zone of the future shear fracture of length h.

In Fig. 5a, h corresponds to the length of the shear fracture in Fig. 2, which extends from the right bottom to the left upper part of Specimen No. 2. The plot demonstrates that the preparation of the shear fracture initiates about 36 min after the start of the experiment ($\dot{\varepsilon} = 3 \times 10^{-6}\ \mathrm{s}^{-1}$) in the central part of the soft inclusion and then extends outwards. At $t = 42$ min the shear fracture formation essentially is completed; only a few barriers are left which count for less than 30% of the fracture length h. During the subsequent deformation ($42 < t < 62$ min) only two further fracture events occur, the last one in the bottom part of the specimen, which leads to unstable slip along the macro-shear fracture. If we assume that each of the fracture events along the shear zone also corresponds to a seismic event, then the existence of a period of "seismic silence" is clearly demonstrated prior to unstable shear along the macro-fracture (Fig. 5b). In comparison, the cracks outside the zone of the future macro-shear are randomly distributed in time until the termination of the experiments (Fig. 5c).

A similar sequence of fracture development is observed for Specimen No. 1 in Fig. 6. Here about 60% of the shear fracture plane is developed after 74 min, while the remaining "unbroken" barriers in the central part kept the applied load and broke only 2 min before the final rupture (Fig. 6a). Again one can discriminate the progressive fracturing distributed randomly in the rock adjacent to the main fracture (Fig. 6c), and the periodic distribution of fracture events which lead to rupture along the main fracture. Although other experiments demonstrate a more complex fracture pattern (several faults may initiate), the tendency for a periodic shear fracture formation both in space and time is always recognized. In this respect, it was of only minor importance if the holes were empty or filled with a material (epoxy) of different elastic properties. Similarly, the shape of the inclusion region has no significant effect on the sequence of the fault formation.

The experiments also allow us to speculate on two other critical aspects associated with the development of macro fractures. These are the question of the critical crack density prior to crack interaction as well as an estimate of the value

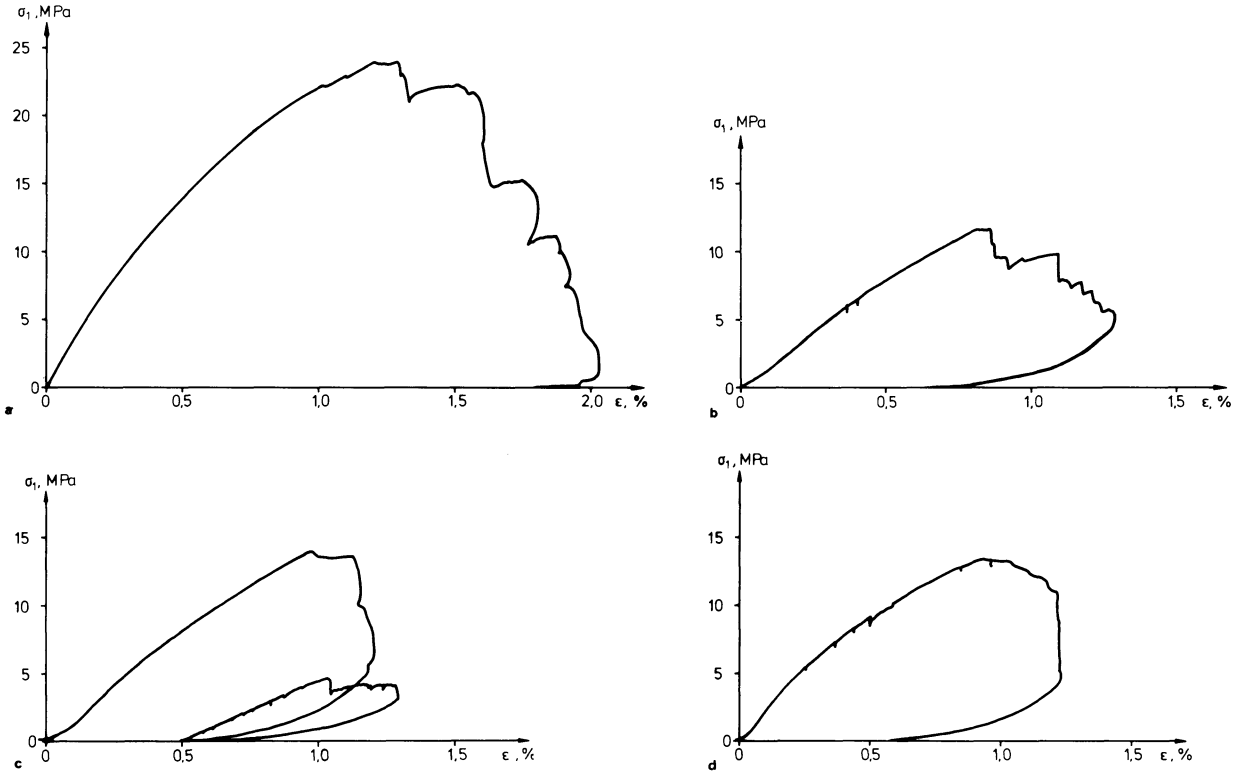

Fig. 4a–d. Stress strain curves: **a** intact specimen; **b** Spec. No. 2 with empty holes in rectangular soft inclusion; **c** Spec. No. 6 with empty holes in elliptical soft inclusion; **d** Spec. No. 8 with epoxy-filled holes in elliptical inclusion. σ_1 axial stress, ε axial strain

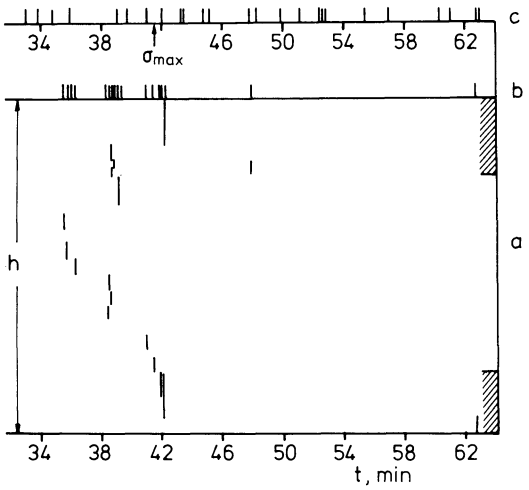

Fig. 5a–c. Fracture development in Spec. No. 2 as a function of space and time t: **a** fracture preparation in the main shear zone of length h; **b** sequence of crack events in the central shear zone; **c** sequence of micro-fracturing outside the main shear fault. σ_{max} peak strength

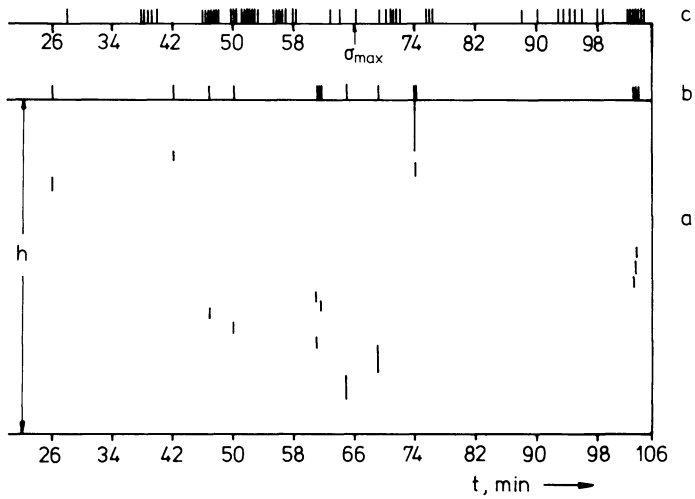

Fig. 6a–c. Spec. No. 1, see caption for Fig. 5

of the critical strain energy release rate or specific surface energy.

In order to estimate the critical crack interaction parameter K mentioned above, we consider the length of cracks within the soft inclusion region and the distance between neighbouring cracks. The average length of visible initial cracks is about $\bar{l}=6$ mm, which also reflects the average distance between the holes. Since large fractures originate from interaction of initial cracks their length is taken as a multiple of the initial crack length. The average distance between neighbouring cracks may be estimated for the 2 D case from $\bar{L}=(S/N)^{1/2}$, where N is the total number of cracks of length $\bar{l}$ and S is the area of the large face of the specimen. Then the evaluation at the moment of unstable shear fracture formation results in K-values for pyrophyllite between 3 and 5 (Table 1). These are of the same

order of magnitude as the values of K observed for technical materials (Zhurkov et al., 1977). K-values derived for specimen failure range from 2 to 3. The only exception is the value for specimen No. 9 ($K=4.9$) which contained only 28 drillholes so that the average distance between cracks was considerable less. If we confine this analysis to the narrow zone around the diagonal macro-shear failure, the K-value may be defined as the ratio between the total length of the unbroken barriers and the length of the broken barriers. This yields a K-value of 0.4–0.5. This may reflect the fact that during the final stage prior to instability the total load is carried by only a few, very strong obstacles, and crack coalescence is negligible.

The critical energy release rate G_c is defined such that $G_c \delta f$ is the *excess of work* done by the external forces over the total change in strain energy of the material and the work against frictional forces which resist crack motion (δf area of infinitesimal crack propagation). Physically G_c can be interpreted as the energy flux to breakdown processes at the crack tip. For pure mode-II crack growth under plane strain conditions G_{IIC} is related to the critical stress intensity factor K_{IIC} by

$$G_{IIC}=\frac{1-\nu^2}{E}K_{IIc}^2 \tag{2}$$

where E is the Young's modulus and ν the Poisson ratio. An estimate of the magnitude of the fracture energy G_{IIC} for fault motion where cracking is not only confined to the crack tip region, can be obtained from the slip-weakening model suggested by Rice (1980). The model assumes that the shear strength τ of the material resisting slip varies with the amount of slip, Δs and the excess of the actual work of the breakdown process over the work of frictional sliding against the residual stress τ_r corresponds to the mode-II critical energy release rate G_{IIC} and is given by the relation

$$G_{IIC}=\int_0^{\Delta s^*}\{\tau(\Delta s)-\tau_r\}\,d(\Delta s). \tag{3}$$

In the simplest case the breakdown process is modelled as rate insensitive and τ exhibits a peak strength τ_m which degrades to a constant residual friction level, τ_r, when Δs exceeds an amount Δs^*. The peak strength τ_m may correspond to the onset of slip for fresh fracture, but perhaps preceeded by slip at lower stress levels for a pre-existing fault.

Although Eq. (3) relates to *local* shear events at stress concentrations along a potential shear plane, Rice (1980) suggested that G_{IIC}-values should be estimated from macroscopic unstable stick-slip events in laboratory triaxial compression experiments on specimens containing polished sawcut faults (Rummel et al., 1978). In such experiments the slip event occurs in an essentially simultaneous manner everywhere on the fault surface, rather than in a cracklike mode as assumed in Eq. (3). Similarly, we may derive fracture parameters from uniaxial compression tests as carried out within this study on pyrophyllite (Fig. 4, Table 1). For this purpose we must express axial stress σ_1 and strain $\Delta l/l$ in terms of τ and Δs on the shear plane which is inclined at an angle θ with respect to σ_1 (Fig. 7).

For a first rough estimation of G_{IIC} and K_{IIC} values from our experimental data we neglect pre-peak microfracturing and assume that the shear fracture developed during only one instability event when the peak shear strength was reached. This situation is typical for fracture in brittle rocks and generally leads to zero residual strength ($\tau_r=0$) in uniaxial compression tests, particularly if carried out in soft loading systems. As seen from Fig. 4 the fracture behaviour of pyrophyllite is brittle although the fast-acting servo-system prevented an immediate stress drop to $\tau_r=0$. So, taking $\theta\approx 55°$, $E\approx 2$ GPa, $\tau_r=0$ and assuming $\nu=0.3$ we obtain with Eqs. (2) and (3) the results given in Table 2. The average value of G_{IIC} is 8.3 kJm^{-2}, the average value of K_{IIC} is 4.2 MNm$^{-3/2}$. These values are considerable less than the data determined for frictional slip on granite shear surfaces under high normal stresses ($G_{IIC}\approx$ 40–70 kJm^{-2}; Rummel et al., 1978; Rice, 1980). In comparison, Husseini et al. (1975) derived values of G_{IIC} associated with the arrest of earthquake ruptures which range from 1 to 10^6 Jm^{-2}. They divide results into those for frictional sliding (1–10^4 Jm^{-2}) and for fresh fracture (10^4–10^6 Jm^{-2}).

Certainly, the assumption that the shear fracture develops during only one event is correct only for compression tests carried out in soft loading systems which provide sufficient energy for fracture growth. As seen in our experiments using a fast-acting servo-controlled loading system (Fig. 4) the formation of the main fracture is associated with several distinct stress drops of about 0.4–2 MPa or even smaller. For such events the magnitude of G_c ranges from about 0.01 to 2 kJm^{-2} with an average of about 0.2 kJm^{-2} if we estimate the corresponding local slip amount from the

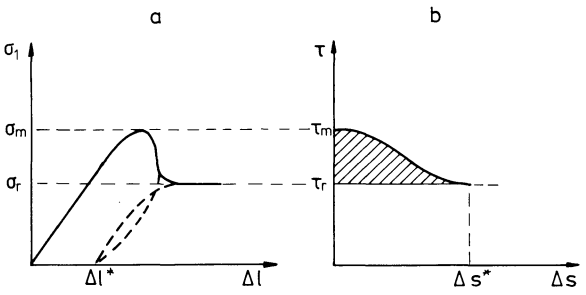

Fig. 7a and b. Procedure inferring shear stress τ and shear displacement Δs from axial stress-strain curves σ_1 vs. Δl. σ_r and τ_r residual strengths. Δl^* irriversible specimen shortening. Shaded area in **b** corresponds to G_{IIC} (after Rice 1980)

Table 2. Fracture energy G_{IIC} and critical stress intensity factor K_{IIC}

Specimens number	Δs^* mm	$\Delta\tau$ MPa	G_{IIC} kJm^{-2}	K_{IIC} MNm$^{-3/2}$
1	3.4	6.9	12	5.1
2	2.1	5.5	5.8	3.6
3	1.5	5.4	4	3.0
4	2.6	6.7	8.7	4.4
5	1.8	8.7	7.8	4.1
6	1.7	6.4	5.4	3.4
8	1.5	6.3	4.7	3.2
9	2.9	5.4	7.8	4.1
10	3.05	8.8	13.4	5.4
12	2.4	6.7	8.2	4.2
7	2.4	11.2	13.7	5.5
average			8.3	4.2

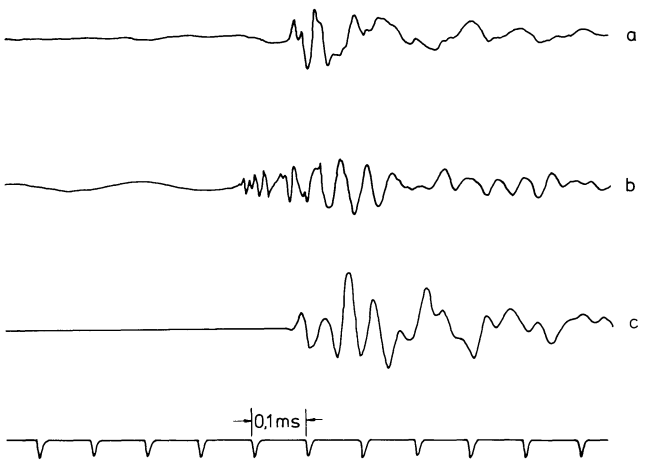

Fig. 8a–c. Examples of typical acoustic emission events monitored by a transient recorder during fracturing in **a** Spec. No. 7, and **b, c** No. 10

axial stress-strain curves as indicated in Fig. 7. This may include considerable errors and therefore the low values of G_{IIC} obtained from small stress drop events should be considered with caution.

Acoustic Emission and Seismic Velocity Changes

As mentioned above, detectable acoustic emission activity was mainly associated with shear fracture development in the specimens. Some examples of acoustic emission signals are given in Fig. 8. The frequency of *P*-waves as 20–100 kHz, decreasing with progressive fracture. The frequency range corresponds to fracture lengths of 6–30 mm. Since only one channel was used, the determination of *S*-wave arrivals is difficult and a source location as well as a discrimination of events from the shear fracture and the surrounding rock was not possible. Thus, Fig. 9 shows only the total number $\bar{N}$ of seismic events as a function of time or strain ($\dot{\varepsilon}=3\cdot10^{-6}\ s^{-1}$), together with the change of stress σ_1, the change of seismic velocities v_p and v_s, and the increase in the number of visible cracks, N. Acoustic emissions appear close to the peak stress when shear fractures initiate. Generally, one shear fracture occurence produced hundreds of recorded events although it is recognized that the counter was triggered continuously during the duration of such a progressive fracture. Thus, only a rough correlation exists between the number of visible cracks and the number of seismic events monitored. Acoustic emission activity was periodic and correlated well with distinct stress drops. No defined period of silence in acoustic emissions prior to the unstable shear fracture propagation is observed. This is apparently due to the fact that shear fractures occur randomly outside the main fracture before instability (seismic silence, Fig. 5c, 6c).

Both *P*- and *S*-wave velocities measured along the σ_1-direction increased considerably during the elastic stage of loading (Fig. 9). The *S*-wave velocity starts to decrease after the first shear fracture appears. *P*-wave velocities tend to decrease only in the post-failure region. The ratio v_p/v_s seems to increase during the final stage of the experiments.

Conclusions

The experiments clearly demonstrate that fracture processes will be confined to a soft inclusion in brittle rock, if locations of high stress concentrations exist in this region. Volumetric cracking in the form of tensile cracks is stable and generally randomly distributed. Crack interaction starts from more complex cracks which subsequently often appear at locations of initially highest compression. Theoretical studies to investigate the changes in the local stress field due to first cracking are urgently needed to understand the origin of these secondary cracks. The crack interaction leads to the formation of a macro-shear fracture. The crack interaction parameter for the total specimen volume has the same value as for many technical materials. But it is considerable smaller in the area of the shear fracture zone. This indicates that the total applied load is carried by only a small number of strong barriers in the shear fracture zone during the final stage of macro-shear fracture formation. This stage may be interpreted as the period of seismic silence and the barriers as seismic gaps in the sequence of earthquake occurence along seismo-active natural faults.

The values obtained for the fracture energy of the pyro-

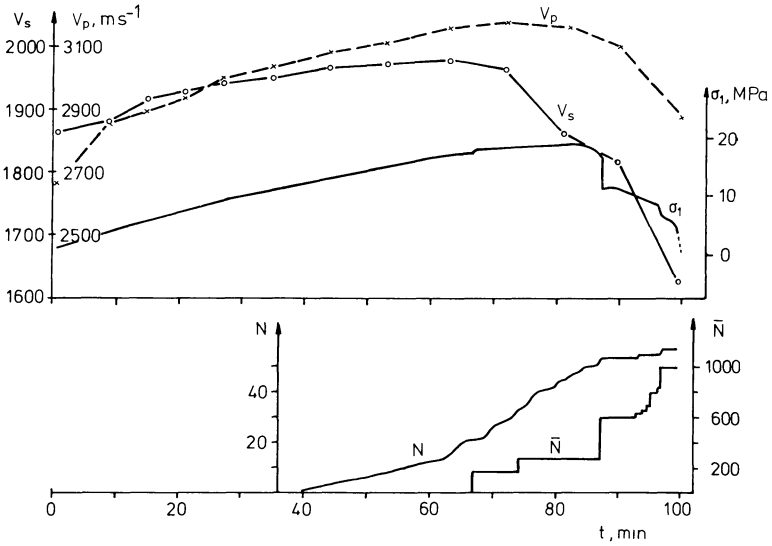

Fig. 9. Axial stress σ_1, *P*- and *S*-wave velocity v_p and v_s, number of visible cracks, N, and number of acoustic emission events $\bar{N}$ as a function of time during deformation of Spec. No. 10

phyllite rock investigated are in the range of values discussed for frictional sliding associated with the arrest of earthquake ruptures ($1–10^4$ Jm^{-2}; Husseini et al., 1975) and do not account for fresh fracture ($10^4–10^6$ Jm^{-2}). However, it must be realized that pyrophyllite is a rock of low strength and, although brittle under uniaxial deformation, will deform easily by discrete shear under moderate confining stresses. Since only a few direct measurements for determining values of fracture energy of mode-II behaviour exist it seems necessary to systematically investigate this parameter for a large range of rocks. Simultaneously, we carefully must consider the techniques and boundary conditions in such experiments. Similarly, the question of stress drop, and shear fracture growth or confined slip on existing faults urgently need further quantitative experimental research.

Although numerous theoretical approaches exist and this study revealed some first empirical information on shear localization, it seems important to further quantify experimental observations, particularly in coarse grained rocks without artificial strain concentrators as well as under various environmental conditions such as stress confinement, temperature and pore fluids. Simultaneously, volumetric fracturing should be considered as it permits pore pressure changes and the migration of fluids prior to earthquakes.

Acknowledgements. The experimental studies were carried out during a visit by G. Sobolev to the Institute of Geophysics, Ruhr-University Bochum in February 1982. Part of the sample preparation and some preliminary tests were made earlier at the Institute of Physics of the Earth, Academy of Science, Moscow, USSR. The authors thank Th. Wöhrl for technical assistance in the experiments and both the Academy of Science USSR and the German Science Foundation for arranging the exchange visits.

References

Brace, W.F., Byerlee, J.D.: Stick-slip as a mechanism for earthquakes. Science **153**, 990–1002, 1966

Haskell, N.. Total energy and energy spectral density of elastic wave radiation from propagating faults. Bull. Seismol. Soc. Am. **54**, 1811–1841, 1964

Haskell, N.. Total energy and energy spectral density of elastic wave radiation from propagating faults. Part II. A statistical source model. Bull. Seismol. Soc. Am. **56**, 125–140, 1966

Hsu, S.-H.: Characteristics of the Haicheng earthquake of 1975. Jet Prop. Lab. CalTech., JPLSP 43-32, Proc. of Lectures by Seism. Del. PRC, 20–29, 1976

Husseini, M.I., Javanovich, D.B., Randall, M.J., Freund, L.B.: The fracture energy of earthquakes. Geophys. J.R. Astron. Soc. **43**, 367–385, 1975

Kostrov, B.V.: Mechanics of the tectonic earthquake source. Moscow: Nauka, 1975

Lockner, D., Byerlee, J.D.: Hydrofracture in Weber sandstone at high confining pressure and differential stress. J. Geophys. Res. **82**, 2018–2026, 1977

Madariaga, R.: Dynamics of an expanding circular fault. Bull. Seismol. Soc. Am. **66**, 639–666, 1976

Madariaga, R.. High-frequency radiation from crack (stress-drop) models of earthquake faulting. Geophys. J.R. Astron. Soc. **51**, 625–651, 1977

Mogi, K.: Source locations of elastic shocks in fracturing process in rocks. Bull. Earthquake Res. Inst. **46**, 1103–1125, 1968

Muskhelishvili, N.I.: Some basic problems of the mathematical theory of elasticity. 4th edition. Groningen: Noordhoft 1953

Myachkin, V.I., Kostrov, B.V., Sobolev, G.A., Shamina, O.G.: Laboratory and theoretical investigations of earthquake preparation. Reports Acad. Sci. USSR, Physics of the Earth **10**, 107–112, 1974

Myachkin, V.I., Brace, W.F., Sobolev, G.A., Dieterich, J.H.: Two models of earthquake forerunners. Pageophys **113**, 169–181, 1975

Nersesov, I.L., Teitelbaum, U.M., Ponomarev, V.S.: Weak seismicity activation as earthquake precursor. Rep. Acad. Sci. USSR **249**, 1335–1338, 1979

Rice, J.R.: Theory of precursory processes in the inception of earthquake rupture. Gerlands Beitr. Geophys **88**, 91–127, 1979

Rice, J.R.: The mechanics of earthquake rupture. In: Physics of the Earth's Interior (Proc. Int. School of Physics, Enrico Fermi Course 78, 1979), A.M. Dziewonski and E. Boschi, eds.. pp. 555–649. Ital. Phys. Soc., North Holland Publ. Co. 1980

Rudnicki, J.W.: Fracture mechanics applied to the earth's crust. Ann. Rev. Earth Planet. Sci. **8**, 489–525, 1980

Rummel, F., Fairhurst, C.: Determination of the post-failure behaviour of brittle rock using a servo-controlled testing machine. Rock Mech. **2**, 189–204, 1970

Rummel, F.: Experimentelle Untersuchungen zum Bruchvorgang in Gesteinen. Berichte Inst. Geophys., Ruhr-Univ. No. 4, 1975

Rummel, F., Alheid, H.-J., Frohn, C.. Dilatancy and fracture induced velocity changes in rock and their relation to frictional sliding. Pageoph **116**, 743–764, 1978

Sobolev, G.A., Spetzler, H., Salov B.: Precursors to failure in rocks while undergoing anelastic deformations. J. Geophys. Res. **83**, 1775–1784, 1978

Sobolev, G.A., Spetzler, H., Koltzov, A.V., Sondergeld, C.: Ultrasonic fracture radiation in rock specimens under deformation. Rep. Acad. Sci. USSR, Physics of the Earth **11**, 33–44, 1980

Sobolev, G.A., Zavialov, A.D.: A concentration criterium for seismoactive faults. Earthquake Prediction. An Intern. Review. A.G.U., Washington, 377–380, 1981

Talwani, P.: Earthquake prediction studies in South Carolina. Earthquake Prediction. An Intern. Review,. A.G.U., Washington, 381–393, 1981

Wawersik, W.R.. Detailed analysis of rock failure in laboratory compression tests. PhD-Thesis, Univ. Minnesota, 1968

Zhurkov, S.N., Kuksenco, V.S.. To rock failure prediction. Rep. Acad. Sci. USSR, Physics of the Earth 6, 11–18, 1977

Received April 7, 1982; Revised version August 30, 1982; Accepted August 31, 1982